Chemical Science

ROYAL SOCIETY OF CHEMISTRY

EDGE ARTICLE

View Article Online
View Journal

Cite this: DOI: 10.1039/d6sc02610a

All publication charges for this article have been paid for by the Royal Society of Chemistry

Inducing configurational stability in inherently flexible expanded heterohelicenes and unlocking stimuli-responsive chiroptical switching

Manisha Pal, †[a] Pirudhan Karak, †[a] Debranjan Hati,[b] Mrityunjay Giri,[a] Subi J. George *[b] and Joyanta Choudhury *[a]

"π-Expanded" (hetero)helicenes have attracted special attention by virtue of their increased helical diameter, enlarged cavity, structural flexibility, and dynamics. However, their structural flexibility results in low enantiomerization barriers ($\Delta G_e^{\ddagger}$ < 20 kcal mol^{-1}), imposing a significant challenge to their enantiomeric separation, and hence, the study of their chiroptical properties. Therefore, there is a rising interest in increasing the $\Delta G_e^{\ddagger}$ of "π-expanded" (hetero)helicenes to enable their chiral separation and chiroptical study. Previously, we disclosed a new type of expanded poly-aza[9]helicenes that possess low $\Delta G_e^{\ddagger}$ (17–18 kcal mol^{-1}) values at 25 °C, and thus, their *P* and *M* enantiomers are difficult to separate, suggesting the necessity of suitable structural modification. Herein, addressing this problem, we report the synthesis of configurationally-stable analogues of the expanded poly-aza[9]helicenes by introducing bulky *tert*-Bu groups at the terminal overlapping rings to restrict ring-flapping. The $\Delta G_e^{\ddagger}$ values for these compounds are significantly higher (>35 kcal mol^{-1}), allowing *P*/*M* enantiomer separation *via* chiral-HPLC. They show a g_{abs} of $\pm 3 \times 10^{-3}$ and g_{lum} of $\pm 5 \times 10^{-3}$, and have stable chiroptical properties at elevated temperatures. Moreover, the basic imidazole units within these novel poly-aza[9]helicenes enable pH-responsive chiroptical switching. Overall, the stable chiroptical property and stimuli-responsive chiroptical function of this class of expanded poly-aza[9]helicenes could make them promising candidates for potential chirality-based applications.

Received 30th March 2026
Accepted 10th April 2026

DOI: 10.1039/d6sc02610a

rsc.li/chemical-science

Introduction

Helicenes are among the class of "molecules in distress",[1] as they "suffer" from significant steric strain between the terminal rings of their winding structure, leading to a conformational distortion of the π-conjugated polycyclic arene framework. However, this "suffering" is complemented by chirality, one of the most intriguing properties in chemical structures, stemming from the handedness of their helical shape. It is this chirality that endows the helicenes with fascinating chiroptical properties such as circular dichroism (CD) and circularly polarized luminescence (CPL). A variety of emerging (opto) electronic applications are associated with efficient CD/CPL properties, and consequently, there is an extensive research interest in developing helicene compounds that are suitable as materials for such applications.[2] For practical applications, configurational stability with a high racemization barrier is the basic requirement.[3] There have been several developments in the world of archetypal helicenes (possessing only angularly/*ortho*-fused rings along the helical backbone) toward isolating enantiopure compounds and studying their chiroptical properties (Fig. 1A), which have led to cutting-edge applications in materials science.[1b,c,4] Very recently, a novel class of helicenes, called "expanded" (possessing both linearly- and angularly-fused rings along the helical rim) carbohelicenes (all-carbon helicenes)/heterohelicenes (heteroatom/s-containing helicenes) have been introduced in this field, with enriched structural diversity, modulated electronic and optoelectronic properties, dynamic chirality, and superior chiroptical properties (Fig. 1A).[5] However, the inherent flexibility in these expanded versions, owing to their enlarged helical diameter, complicates the separation/isolation of the enantioenriched compounds and the study of their chiroptical properties because of their low $\Delta G_e^{\ddagger}$ values ($\Delta G_e^{\ddagger}$ < 20 kcal mol^{-1}) (Fig. 1A and B). Therefore, commonly employed strategies to obtain enantiomerically pure expanded helicenes at ambient temperatures with high $\Delta G_e^{\ddagger}$ values ($\Delta G_e^{\ddagger}$ > 35 kcal mol^{-1}), are: (a) increasing the length of the helical chain, (b) π-extension at the periphery of the helicenes, (c) multiplexing helicenic motifs on the same parent helicene backbone, and (d) bulky group substitution at the

[a]*Organometallics & Smart Materials Laboratory, Department of Chemistry, Indian Institute of Science Education and Research (IISER) Bhopal, Bhopal 462 066, India. E-mail: joyanta@iiserb.ac.in*

[b]*New Chemistry Unit, School of Advanced Materials, Jawaharlal Nehru Centre for Advanced Scientific Research (JNCASR), Bangalore 560064, India. E-mail: george@jncasr.ac.in*

† M. P. and P. K. contributed equally to this work.

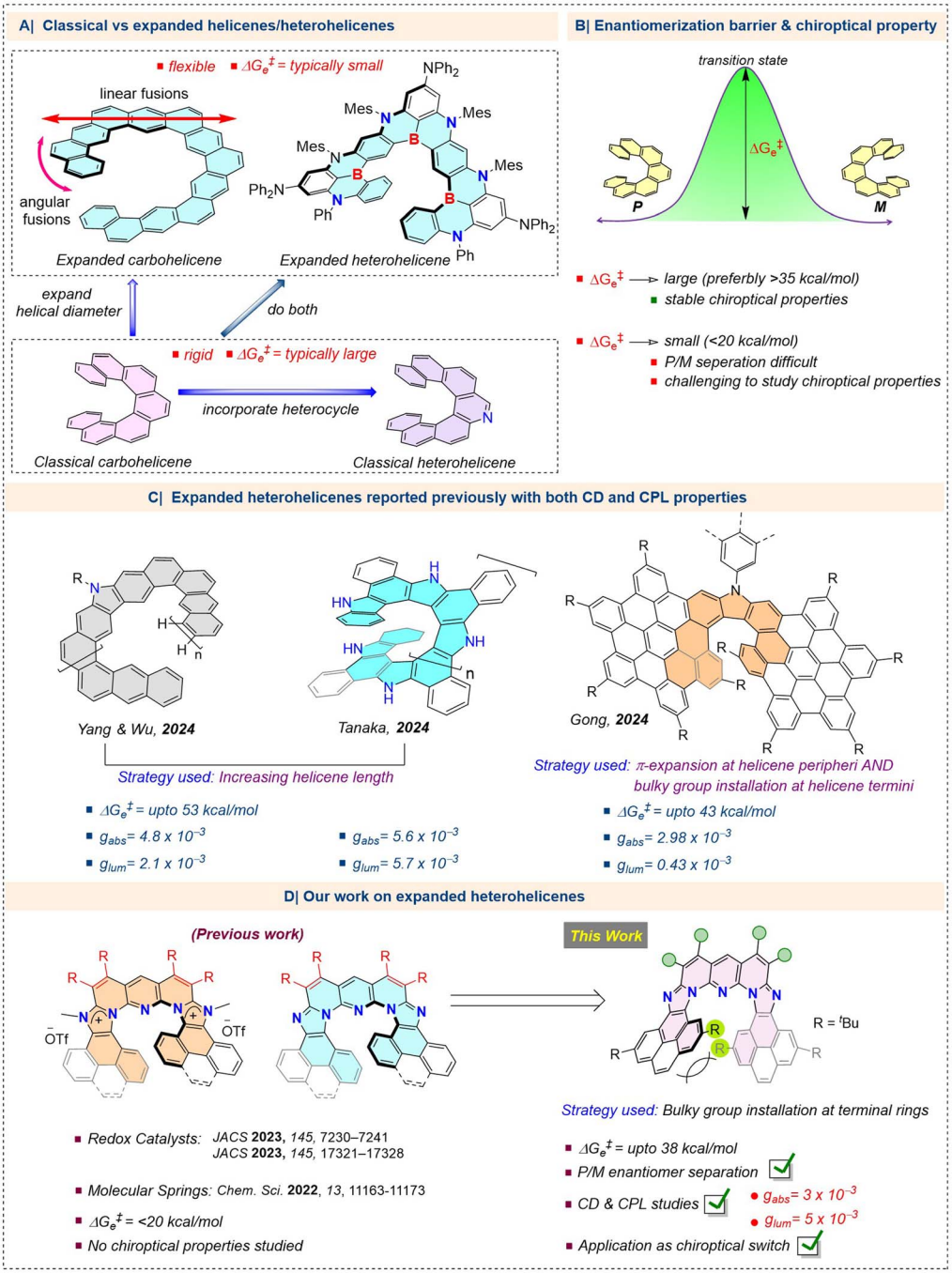

Fig. 1 (A) Examples of classical and expanded (hetero)helicenes. (B) Enantiomerization barrier and chiroptical properties of helicenes. (C) Examples of reported expanded heterohelicenes and their chiroptical properties. (D) Our earlier work and the key strategy and features of this work on expanded heterohelicenes.

internal or terminal rings of the helical backbone.[5e,6] However, the examples of enantiomerically pure expanded carbohelicenes are limited,[7] and expanded heterohelicenes with a high racemization barrier have been very rare until now.[5f,8,9] Just recently, in 2024, three independent studies by Yang and Wu,[5f] Tanaka,[8a] and Gong,[9] reported expanded heterohelicenes with high $\Delta G_e^{\ddagger}$ values (Fig. 1C). The previously mentioned strategies have been exploited in these works to achieve the required racemization barrier value and hence excellent absorption and luminescence dissymmetry factors. Notably, all of these expanded heterohelicenes possess carbazole as the heterocycle in their helical backbone. Systems incorporating electronically diverse heterocycles are highly desired in order to explore their modulated CD/CPL properties and new chiroptical functions such as stimuli-responsive chiroptical switches (*vide infra*).

Recently, we developed a double 'rollover π-expansion' (RoPE) strategy-enabled synthesis of an intriguing class of neutral and cationic "expanded" poly-azahelicenes, embedded

with an imidazole/imidazolium-fused pyridine-based mixed heterocyclic scaffold (Fig. 1D).[10] While the cationic systems were exploited as a novel class of redox-active electrocatalysts for the CO_2-reduction reaction (CO_2RR) and hydrogen evolution reaction (HER),[11] both the neutral and cationic compounds were used as stimuli (pH and light)-controlled soft molecular springs due to their flexible helical backbone.[10b] The same flexibility of these expanded heterohelicenes prevents configurational stability (calculated $\Delta G_e^{\ddagger}$ value < 20 kcal mol^{-1} at 25 °C). We endeavoured to achieve the configurationally stable version of our expanded heterohelicenes by introducing bulky *tert*-butyl groups at the overlapping terminal rings of the helical rim (strategy (d) mentioned above) (Fig. 1D). Consequently, we successfully demonstrated the separation and isolation of the *P* and *M* enantiomers and evaluated the chiroptical properties, and finally, to showcase a potential application, uncovered a highly reversible on/off chiroptical switching function with the enantioenriched compounds by capitalizing on the embedded pH-responsive imidazole moieties (Fig. 1D).

Results and discussion

Synthesis

The precursor for the target helicenes, 2,6-bis(2,7-di-*tert*-butyl-9*H*-pyreno[4,5-*d*]imidazole-9-yl)pyridine (**PYBIM**) was synthesized by the reaction of 2,6-difluoropyridine with 2,7-di-*tert*-butyl-9*H*-pyreno[4,5-*d*]imidazole under basic conditions (Schemes S1–S4; see SI for details). The targeted expanded poly-aza[9]helicenes, **HELI-1** and **HELI-2**, were obtained in good yields (62–73%) by applying our 'rollover π-expansion' protocol

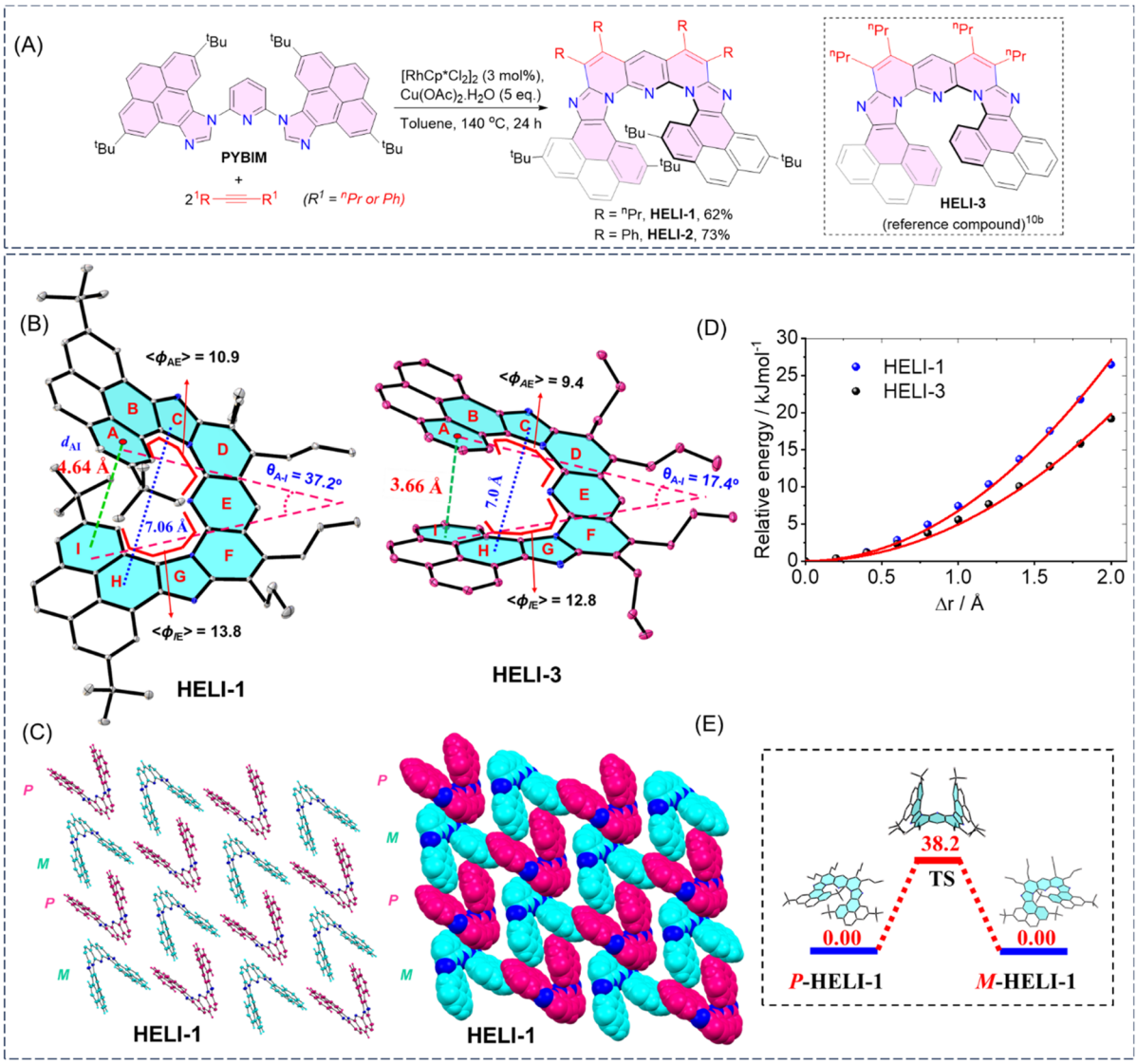

Fig. 2 (A) Synthesis of π-expanded poly-aza[9]helicenes **HELI-1** and **HELI-2**. The reference non-^{t}Bu analogue compound **HELI-3** (reported previously by our group[10b]) is also shown. (B) Crystal structures and comparison of key metric parameters of **HELI-1** (CCDC 2485128) and **HELI-3**. (C) Crystal packing and space-filling diagrams of **HELI-1**, showing the arrangement of the *P*/*M* isomers in the crystalline state. (D) Spring constant plots of **HELI-1** and **HELI-3**.[10b] (E) Enantiomerization energy barrier (kcal mol^{-1}) of **HELI-1**, computed *via* the DFT method (B3LYP/6-311g(2d,p) level of theory). TS = transition state. See SI for details.

with the catalyst $[RhCp^*Cl_2]_2$ on the precursor **PYBIM** with two different internal alkynes (Fig. 2A). The compounds **HELI-1** and **HELI-2** were both well characterized by NMR spectroscopy and mass spectrometry studies (see SI for details).

Crystal structure

The helical structure of **HELI-1** (Fig. 2B) was unambiguously confirmed by single-crystal X-ray diffraction (SCXRD) analysis, using suitable crystals grown by diffusing hexane into a dichloromethane solution of the compound at room temperature. The crystal packing profile revealed alternating stacks of both the *P* and *M* enantiomers aligned along the vertical axis, resulting in a racemic columnar structure (Fig. 2C). At the molecular level, analysis revealed that the helical pitch (d_{AI}), the vertical distance between the two terminal rings of **HELI-1** was 4.64 Å, which was much higher than that of our previously reported non-^{t}Bu expanded heterohelicene analogue **HELI-3** (d_{AI} = 3.66 Å).[10b] The intersecting angle (θ_{AI}) between the two planes passing through the two terminal rings was 37.2°, which is markedly larger than that of **HELI-3** (17.4°). The torsion angles of two helicinic wings were 10.9° and 13.8°, exceeding those observed for **HELI-3** (9.4° and 12.8°). The higher values of the helical pitch, angle, and torsion angles in **HELI-1** were attributed to the presence of the bulky *tert*-butyl groups on the overlapping terminal rings of the helicene rim, which imposed severe steric hindrance between these two rings. Although we could not obtain high-quality single crystals suitable for high-quality diffraction data for **HELI-2** despite several attempts, the gross structure showed similar features to those of **HELI-1** (see SI for details). The above structural characteristics suggested the incorporation of the desired rigidity in the inherently flexible helicenic backbone of the expanded heterohelicenes **HELI-1** and **HELI-2**. Indeed, the molecular spring constant (k) value of **HELI-1** calculated *via* the density functional theory (DFT) method (Fig. 2D and S5 in SI) was found to be 2.25 N m^{-1}, which was significantly higher than that (k = 1.64 N m^{-1}) of **HELI-3**, indicating that the ^{t}Bu groups induced reduction of the flexibility of the helical rim in the former compound. Overall, it appeared that the presence of the bulky ^{t}Bu groups at the two terminal overlapping rings would be able to restrict the easy flapping of the terminal rings to a great extent, and therefore, a high enantiomerization barrier was anticipated. Therefore, we investigated the enantiomerization barrier for **HELI-1** *via* DFT using dichloromethane solvent at 298.15 K (Fig. 2E). The $\Delta G_e^{\ddagger}$ value was found to be 38.2 kcal mol^{-1}, which was expectedly much higher compared to that of **HELI-3** ($\Delta G_e^{\ddagger}$ = 16.5 kcal mol^{-1} at 25 °C), as well as those of many other reported expanded carbo/heterohelicenes, such as expanded [13]-helicene[5c] ($\Delta G_{e\ theory}^{\ddagger}$ = 13.0 kcal mol^{-1} at 25 °C), the aza-bora [9]-helicene[7a] ($\Delta G_{e\ theory}^{\ddagger}$ = 14.3 kcal mol^{-1} at 25 °C) and [7]-heliphene[12] ($\Delta G_{e\ experimental}^{\ddagger}$ = 12.6 kcal mol^{-1} at −27 °C). Similarly, the DFT -calculated enantiomerization barrier of **HELI-2** was found to be 39.1 kcal mol^{-1} (Fig. S4, SI), which is comparable to that of **HELI-1**.

Chiroptical properties

The sufficiently high $\Delta G_e^{\ddagger}$ value indicated the possibility of chiral resolution of the *P* and *M* enantiomers of these new expanded poly-[9]azahelicenes. We first chose **HELI-2** for investigating chiral resolution and follow-up chiroptical properties. After a thorough screening of conditions, the *P* and *M* enantiomers of **HELI-2** were successfully resolved *via*

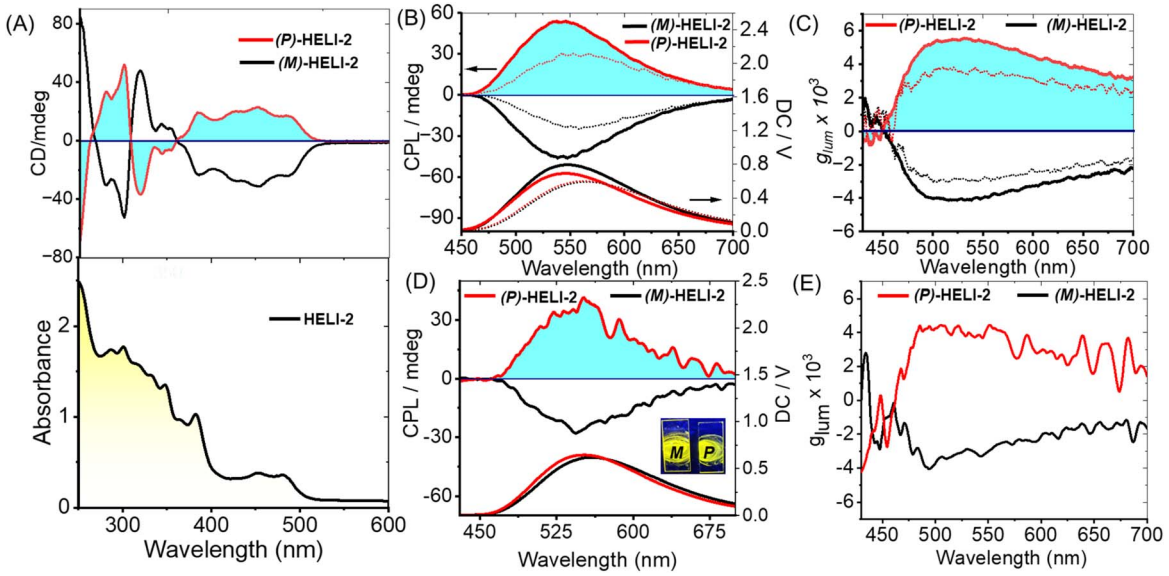

Fig. 3 (A) Absorption (bottom) of HELI-2 and mirror image CD (top) spectra of (*P*/*M*)-HELI-2 in hexane (18.0 μM). (B) Mirror image CPL spectra (top; with left-hand-side *Y*-axis) and corresponding direct current (DC) spectra (bottom; with right-hand-side *Y*-axis) of (*P*/*M*)-HELI-2 in hexane (solid line) and in DCM (dotted line) (18.0 μM). (C) Luminescence dissymmetry factors of (*P*/*M*)-HELI-2 in hexane (solid line) and in DCM (dotted line); excitation: 330 nm. (D) Mirror image CPL spectra (top; with left-hand-side *Y*-axis) and corresponding DC spectra (bottom; with right-hand-side *Y*-axis) of (*P*/*M*)-HELI-2 in solid thin film. (E) Luminescence dissymmetry factors of (*P*/*M*)-HELI-2 in solid thin film.

chiral HPLC using a Daicel CHIRALPAK IA-3 column and *n*-hexane/^{i}PrOH (90 : 10, v/v) as the eluent (Fig. S7, SI). The chiroptical properties and performances of the isolated *P*/*M* enantiomers were evaluated in both solution and solid state (thin film) using both CD and CPL studies.

The UV-vis absorption and CD spectra of the isolated enantiomers (*P*/*M*) of **HELI-2** are shown in Fig. 3A. The compound showed intense absorption bands at 350–375 nm and 430–500 nm ($\varepsilon = 54\,510\ M^{-1}\ cm^{-1}$ at 355 nm; $\varepsilon = 19\,800\ M^{-1}\ cm^{-1}$ at 445 nm in DCM; Fig. S9, SI). The absolute configuration of *P*/*M*-**HELI-2** was determined by comparing the experimental and simulated CD spectra (calculated using the DFT method, Fig. S65, SI). The CD spectra of the two enantiomers as expected, showed mirror-imaged bisignate signals between 250 nm and 550 nm (the *P* and *M* isomers showed positive and negative ECD, respectively, at the absorption onset). The *P*/*M*-**HELI-2** enantiomers displayed high absorption dissymmetry factors ($g_{abs} = \Delta\varepsilon/\varepsilon$) of $\pm 3 \times 10^{-3}$ in hexane at 425 nm (Fig. S15, SI), similar to those of many large π-extended helicenes.[5e] The linear dichroism (LD) experiments (Fig. S17 in the SI) ruled out any LD contribution to the observed chiroptical properties, implying that there is no macroscopic alignment of the chromophore under the experimental conditions in either hexane or dichloromethane. This is also supported by rotation-dependent CD spectra (Fig. S16 in SI), where similar spectral features were observed with rotation. **HELI-2** showed strong fluorescence in the 490–680 nm range with $\lambda_{max} = 560$ nm in DCM solution (Fig. S9b, SI) and $\lambda_{max} = 555$ nm in hexane solution. The fluorescence quantum yield was calculated to be 0.38 and 0.30 in DCM and hexane, respectively (Table S4, SI). In the DC spectra, $\lambda_{max} = 560$ nm matches the emission spectra (Fig. 3B). The *P*/*M*-**HELI-2** showed mirror image CPL spectra with $\lambda_{max} = 550$ nm in hexane and $\lambda_{max} = 560$ nm in DCM, which matches both the emission and DC spectra (Fig. 3B). The CPL dissymmetry factor (g_{lum}) was measured to be $\pm 5 \times 10^{-3}$ in hexane, and $\pm 3 \times 10^{-3}$ in dichloromethane (Fig. 3C), which seems to be promisingly high and comparable to those of other relatively rigid carbo/heterohelicenes.[5e,f,9,13] As **HELI-2** was sparingly soluble in hexane, molecular aggregation occurred, which resulted in a higher g_{lum} value.[13] The dynamic light scattering (DLS) data (Fig. S18 in SI) also suggested that the particle size is larger in hexane solution compared to that in DCM. Interestingly, the *P* and *M* isomers of **HELI-2** also showed emission in the solid-state (Fig. 3D), and accordingly, they displayed mirror-image CPL profiles in the solid-state (drop-cast film), with a high g_{lum} value of $\pm 4 \times 10^{-3}$ (Fig. 3E). Thus, based on these encouraging chiroptical performance parameters, the *P* and *M* **HELI-2** enantiomers exhibited potential for further practical solid-state applications.

Similarly, **HELI-1** exhibited absorption bands at 320–370 nm and 420–500 nm ($\varepsilon = 59\,900\ M^{-1}\ L\ cm^{-1}$ at 345 nm; $\varepsilon = 17\,600\ M^{-1}\ L\ cm^{-1}$ at 435 nm in DCM; Fig. S8, SI). The chiral resolution of **HELI-1** was also achieved, and the corresponding *P* and *M* enantiomers displayed mirror-image CD and CPL spectra (Fig. S12 and S13 SI). For **HELI-1**, the g_{abs} and g_{lum} values are found to be $\pm 4 \times 10^{-3}$ and $\pm 5 \times 10^{-3}$, respectively, in DCM (Fig. S12–S14, SI).

Temperature-dependent chiroptical properties

The stable chiroptical properties of these compounds at high temperatures reinforced their suitability for further practical applications. As hexane or DCM are low-boiling solvents, toluene and *ortho*-dichlorobenzene were used for studying their temperature-dependent chiroptical properties. Before performing the experiment, we confirmed that **HELI-2** was in monomeric form in toluene *via* a DLS study (Fig. S18 in SI), and ensured that similar chiroptical properties to those in DCM solvent were retained (Fig. S23 in SI). The variation of the CD signal at 450 nm as a function of temperature was measured in toluene with a temperature gradient of 10 °C/50 min (Fig. S24–S29 in SI). No change in the CD signal was observed up to 75 °C with increasing temperature (Fig. 4A), which supported the high $\Delta G^{\ddagger}_{e}$. In CP-OLEDs, chiral emitters often face heating-related issues that can affect their stability and performance during operation. Therefore, the retention of CPL properties at high temperatures is essential. Thus, we also measured variable-temperature CPL, and no change in λ_{max} (550 nm) or CPL signal intensity was evident for either of the isomers (Fig. 4B, and S38–S43 in SI) in the 25–75 °C range. The g_{lum} value also remained constant up to 75 °C (Fig. S44 in SI). It is notable that we did not observe the decay of the CD or CPL signal in toluene solution up to 75 °C. Similarly, when *ortho*-dichlorobenzene was

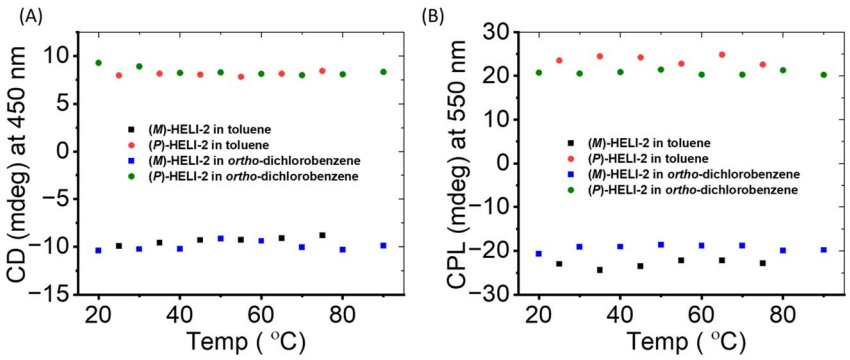

Fig. 4 (A) Change in the CD signal (at 450 nm) and (B) CPL signal (at 550 nm) of (*P*/*M*)-**HELI-2** with temperature in toluene and *ortho*-dichlorobenzene solution (concentration = 8 μM).

used as the solvent, the CD and CPL properties were retained up to 90 °C (Fig. S30–S37 and S45–S52 in SI).

In addition, we verified the stability of the representative chiral (*M*)-**HELI-2** under constant external heating at 160 °C for up to 12 h, using *ortho*-dichlorobenzene as the solvent, and monitored the CD signal at 2-hour intervals. Notably, no detectable decrement in the CD signal was observed, which further confirmed the high racemization barrier value of these expanded helicenes (Fig. S54, SI). On that note, previously, Nowak-Król and coworkers reported azaborathia[9]helicene **H_1-Me_4**, with a racemization barrier of 39.1 kcal mol^{-1}, but no racemization was observed at 170 °C in the solvent *ortho*-dichlorobenzene.[2f]

Furthermore, the half-life ($t_{1/2}$) of the helical inversion process of **HELI-2** was evaluated at different temperatures using the DFT method (Table S2, SI). At 25 °C, the $t_{1/2}$ value was found to be very high ($\sim 10^8$ years); only at very high temperatures, such as at 300 °C, the $t_{1/2}$ value is around 5.34 minutes. This clearly indicates that the racemization of **HELI-2** can be achieved only at very high temperatures, which is experimentally very challenging.

Stimuli-responsive chiroptical switching

As mentioned earlier, owing to the presence of the embedded pH-responsive imidazole moieties, this new class of expanded poly-aza[9]-helicenes opened up the opportunity to explore a stimuli (acid/base)-controlled on/off chiroptical switching function with the *P*/*M* enantiomers.[14] Thus, consecutive treatment of an acid (triflic acid, CF_3SO_3H) and a base (triethylamine, Et_3N) with a solution of **HELI-2** (Fig. 5A) was first monitored *via* UV-vis absorption and fluorescence spectroscopy (Fig. S55, SI). Upon protonation, both the absorption and the emission bands of **HELI-2** red-shifted from 446 nm to 514 nm and from 560 nm to 663 nm, respectively, as the LUMO was stabilized upon protonation (Fig. S62, SI). In the TD-DFT calculated UV-vis spectra, a similar red shift was present (Fig. S63, SI). Moreover, the protonation process was also monitored using ^{1}H NMR spectroscopic studies (Fig S60, SI). The emission intensity of the protonated **HELI-2** was reduced fivefold (Fig. S55 in SI). The original spectral profiles (both absorption and emission profiles) could be regenerated upon deprotonation by the addition of triethylamine (Fig. 5B and S55 in SI). Next, the pH-responsive reversible behavior was examined with the chiral *P*/*M*-**HELI-2** isomers and monitored using CD and CPL spectroscopy. The CD spectra of the *P*/*M*-**HELI-2** isomers also showed changes, with red-shifted (by 30–40 nm) peaks. Less-intense bands were observed at 350 nm and 488 nm for the protonated *P*/*M*-**HELI-2** (Fig. 5B). Upon protonation, a red shift in DC spectra was observed (Fig. 5C). The CPL signal at $\lambda_{max} = 560$ nm in DCM was found to be shifted to $\lambda_{max} \sim 655$ nm with much less CPL intensity when *P*/*M*-**HELI-2** isomers were treated with triflic acid (Fig. 5C). Interestingly, upon the addition of triethylamine, the CPL characteristics were reversibly retained (Fig. 5C), very similar to previously reported N-doped octagon-containing hexabenzocoronene (HBC) system.[14c] The acid–base responsive reversible switching behavior was also confirmed by monitoring the g_{lum} parameter of both the enantiomers (Fig. 5D); upon protonation, the g_{lum} value was found to be reduced to $\sim 10^{-4}$. The above results demonstrated a significant stimulus-controlled chiroptical switching capability of chiroptically stable enantiomers of this new class of expanded poly-azahelicenes, which could be useful for further specialized applications in the field.

In addition, for practical applications, the main requirement is solid-state functionality.[15] Thus, we investigated the acid-base-responsive CPL switching of **HELI-2** in the solid state (drop-cast film). Upon exposure to acid (triflic acid) vapour, the solid-state CPL intensity was found to be decreased significantly. The CPL intensity was recovered upon exposure to base

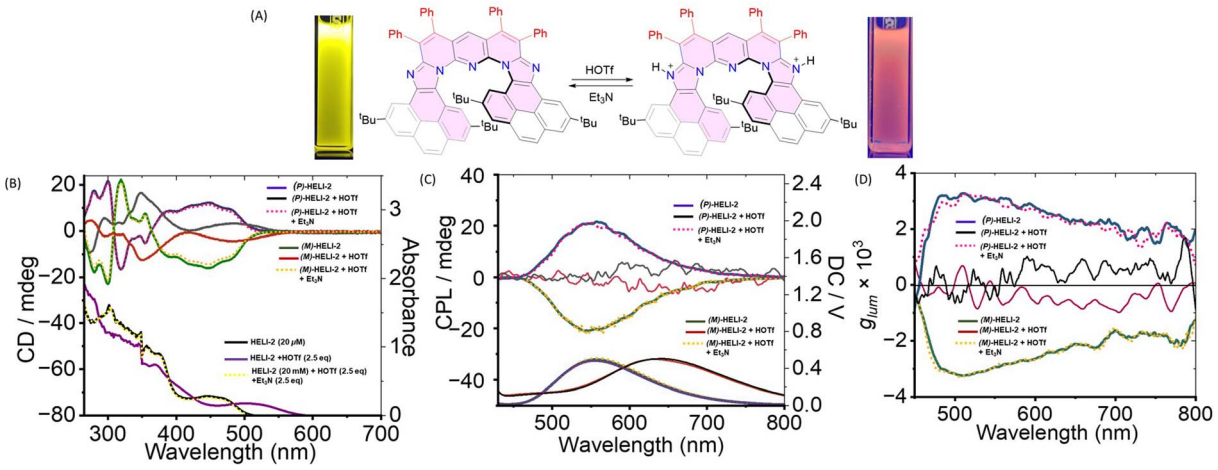

Fig. 5 (A) Acid–base responsive reversible emission properties of **HELI-2** in DCM solution. (B) Absorption (bottom; with right-hand-side *Y*-axis) and CD (top; with left-hand-side *Y*-axis) spectra of (*P*/*M*)-**HELI-2** in DCM (8.0 μM) upon consecutive addition of acid (HOTf) and base (Et_3N). (C) CPL (top; with left-hand-side *Y*-axis) and corresponding DC voltage (bottom; with right-hand-side *Y*-axis) spectra of (*P*/*M*)-**HELI-2** in DCM (8.0 μM) upon consecutive addition of acid (HOTf) and base (Et_3N). (D) Luminescence dissymmetry factors of (*P*/*M*)-**HELI-2** in DCM (8.0 μM) upon consecutive addition of acid (HOTf) and base (Et_3N). $\lambda_{exc} = 330$ nm.

(triethylamine) vapour (Fig. S61, SI), indicating pH control over the CPL output in the solid state. These results demonstrate the viability of stimuli-responsive CPL modulation in solid-state conditions relevant to device applications.

Conclusions

In conclusion, configurationally stable "π-expanded" 9-azahelicenes with a significantly enhanced enantiomerization energy barrier (>38 kcal mol^{-1}) have been synthesized conveniently using a simple catalytic methodology. These unique helicenes can be easily separated into *P* and *M* isomers under ambient conditions. The optically pure chiral helicenes exhibited a high absorption dissymmetry factor g_{abs} ($\pm 3 \times 10^{-3}$ in solution) and luminescence dissymmetry factor g_{lum} ($\pm 5 \times 10^{-3}$ in solution and $\pm 4 \times 10^{-3}$ in solid state), surpassing even those of classical [7]-helicenes. Additionally, the imidazole rings within the helicene core of these molecules endowed them with acid/base-responsive chiroptical switching properties. Crucially, the CPL properties exhibited thermal stability up to 160 °C, indicating their suitability for potential chiral applications.

Author contributions

M. Pal: methodology, investigation, formal analysis, data curation, visualization, writing – original draft; P. Karak: methodology, investigation, formal analysis, data curation, visualization, writing – original draft; D. Hati: investigation, formal analysis, data curation; M. Giri: methodology, investigation; S. J. George: resources, supervision; J. Choudhury: conceptualization, supervision, resources, project administration, funding acquisition, writing. M. Pal, and P. Karak contributed equally to this work.

Conflicts of interest

There are no conflicts to declare.

Data availability

CCDC 2485128 contains the supplementary crystallographic data for this paper.[16]

All data of this research work are available in the manuscript and in the supplementary information (SI). Supplementary information: experimental procedures, computational details, and spectral details. See DOI: https://doi.org/10.1039/d6sc02610a.

Acknowledgements

J. C. thanks the Anusandhan National Research Foundation (ANRF; erstwhile Science and Engineering Research Board, SERB), Government of India (Grant No. CRG/2022/005562), and IISER Bhopal for generous financial support. S. J. G. thanks the ANRF JC Bose Grant (Grant no.: ANRF/2025/02766). M. P. thanks Ministry of Education, Government of India for the award of the Prime Minister's Research Fellowship (PMRF). P. K. acknowledges the Integrated PhD fellowship from IISER Bhopal. D. H. thanks JNCASR for fellowship. The authors acknowledge the extensive use of NMR, Mass, and SCXRD facilities of CIF, IISER Bhopal. The authors gratefully acknowledge the High-Performance Computation (HPC) facility of IISER Bhopal for DFT calculations. The authors would also like to thank the Department of Science and Technology, Government of India for awarding the DST-FIST grant (SR/FST/CS-II/2023/312) to support NMR facilities at IISER Bhopal.

References

1 (*a*) R. Hoffmann and H. Hopf, *Angew. Chem., Int. Ed.*, 2008, **47**, 4474–4481; (*b*) M. Gingras, G. Félix and R. Peresutti, *Chem. Soc. Rev.*, 2013, **42**, 1007–1050; (*c*) M. Gingras, *Chem. Soc. Rev.*, 2013, **42**, 1051–1095.

2 (*a*) K. Dhbaibi, L. Favereau and J. Crassous, *Chem. Rev.*, 2019, **119**, 8846–8953; (*b*) L. Zhang, H.-X. Wang, S. Li and M. Liu, *Chem. Soc. Rev.*, 2020, **49**, 9095–9120; (*c*) V. Kumar, H. J. Bharathkumar, S. D. Dongre, R. Gonnade, K. Krishnamoorthy and S. S. Babu, *Angew. Chem., Int. Ed.*, 2023, **62**, e202311657; (*d*) S. D. Dongre, G. Venugopal, V. Kumar, A. Badrinarayan Jadhav, J. Kumar and S. Santhosh Babu, *Angew. Chem., Int. Ed.*, 2024, e202420767; (*e*) F. Zhang, V. Brancaccio, F. Saal, U. Deori, K. Radacki, H. Braunschweig, P. Rajamalli and P. Ravat, *J. Am. Chem. Soc.*, 2024, **146**, 29782–29791; (*f*) D. Volland, J. Niedens, P. T. Geppert, M. J. Wildervanck, F. Full and A. Nowak-Król, *Angew. Chem., Int. Ed.*, 2023, **62**, e202304291.

3 (*a*) P. Ravat, *Chem.–Eur. J.*, 2021, **27**, 3957–3967; (*b*) J. M. Fernández-García, P. Izquierdo-García, M. Buendía, S. Filippone and N. Martín, *Chem. Commun.*, 2022, **58**, 2634–2645.

4 T. Mori, *Chem. Rev.*, 2021, **121**, 2373–2412.

5 (*a*) G. R. Kiel, S. C. Patel, P. W. Smith, D. S. Levine and T. D. Tilley, *J. Am. Chem. Soc.*, 2017, **139**, 18456–18459; (*b*) Y. Nakakuki, T. Hirose, H. Sotome, H. Miyasaka and K. Matsuda, *J. Am. Chem. Soc.*, 2018, **140**, 4317–4326; (*c*) Y. Nakakuki, T. Hirose and K. Matsuda, *J. Am. Chem. Soc.*, 2018, **140**, 15461–15469; (*d*) A. E. Samkian, G. R. Kiel, C. G. Jones, H. M. Bergman, J. Oktawiec, H. M. Nelson and T. D. Tilley, *Angew. Chem., Int. Ed.*, 2021, **60**, 2493–2499; (*e*) G. R. Kiel, H. M. Bergman, A. E. Samkian, N. J. Schuster, R. C. Handford, A. J. Rothenberger, R. Gomez-Bombarelli, C. Nuckolls and T. D. Tilley, *J. Am. Chem. Soc.*, 2022, **144**, 23421–23427; (*f*) G.-F. Huo, W.-T. Xu, Y. Han, J. Zhu, X. Hou, W. Fan, Y. Ni, S. Wu, H.-B. Yang and J. Wu, *Angew. Chem., Int. Ed.*, 2024, **63**, e202403149.

6 (*a*) P. Ravat, R. Hinkelmann, D. Steinebrunner, A. Prescimone, I. Bodoky and M. Juríček, *Org. Lett.*, 2017, **19**, 3707–3710; (*b*) X. Guo, Z. Yuan, Y. Zhu, Z. Li, R. Huang, Z. Xia, W. Zhang, Y. Li and J. Wang, *Angew. Chem., Int. Ed.*, 2019, **58**, 16966–16972; (*c*) K. Suzuki, H. Fukuda, H. Toda, Y. Imai, Y. Nojima, M. Hasegawa, E. Tsurumaki and S. Toyota, *Tetrahedron*, 2023, **132**, 133243; (*d*) K. Fujise, E. Tsurumaki, G. Fukuhara, N. Hara, Y. Imai and S. Toyota,

Chem.–Asian J., 2020, **15**, 2456–2461; (*e*) Y. Matsuo, S. Seki and T. Tanaka, *Chem. Lett.*, 2024, **53**, upae159.

7 (*a*) J. Full, S. P. Panchal, J. Götz, A.-M. Krause and A. Nowak-Król, *Angew. Chem., Int. Ed.*, 2021, **60**, 4350–4357; (*b*) K. Fujise, E. Tsurumaki, K. Wakamatsu and S. Toyota, *Chem.–Eur. J.*, 2021, **27**, 4548–4552; (*c*) S. Oda, B. Kawakami, Y. Yamasaki, R. Matsumoto, M. Yoshioka, D. Fukushima, S. Nakatsuka and T. Hatakeyama, *J. Am. Chem. Soc.*, 2022, **144**, 106–112.

8 (*a*) Y. Matsuo, M. Gon, K. Tanaka, S. Seki and T. Tanaka, *J. Am. Chem. Soc.*, 2024, **146**, 17428–17437; (*b*) J. Labella, W. R. Osterloh, K. Kuo, Y. Tsutsui, T. Tanaka and S. Seki, *J. Am. Chem. Soc.*, 2026, **148**, 9670–9679.

9 X.-Y. Wang, J. Bai, Y.-J. Shen, Z.-A. Li and H.-Y. Gong, *Angew. Chem., Int. Ed.*, 2025, **64**, e202417745.

10 (*a*) P. Karak, C. Dutta, T. Dutta, A. L. Koner and J. Choudhury, *Chem. Commun.*, 2019, **55**, 6791–6794; (*b*) P. Karak and J. Choudhury, *Chem. Sci.*, 2022, **13**, 11163–11173.

11 (*a*) P. Karak, S. K. Mandal and J. Choudhury, *J. Am. Chem. Soc.*, 2023, **145**, 7230–7241; (*b*) P. Karak, S. K. Mandal and J. Choudhury, *J. Am. Chem. Soc.*, 2023, **145**, 17321–17328.

12 S. Han, A. D. Bond, R. L. Disch, D. Holmes, J. M. Schulman, S. J. Teat, K. P. C. Vollhardt and G. D. Whitener, *Angew. Chem., Int. Ed.*, 2002, **41**, 3223–3227.

13 Z. Qiu, C.-W. Ju, L. Frédéric, Y. Hu, D. Schollmeyer, G. Pieters, K. Müllen and A. Narita, *J. Am. Chem. Soc.*, 2021, **143**, 4661–4667.

14 (*a*) E. Yen-Pon, F. Buttard, L. Frédéric, P. Thuéry, F. Taran, G. Pieters, P. A. Champagne and D. Audisio, *JACS Au*, 2021, **1**, 807–818; (*b*) Y. Matsuo, C. Maeda, Y. Tsutsui, T. Tanaka and S. Seki, *Angew. Chem., Int. Ed.*, 2023, **62**, e202314968; (*c*) M. A. Medel, L. Hortigüela, V. Lloveras, J. Catalán-Toledo, D. Miguel, A. J. Mota, N. Crivillers, A. G. Campaña and S. P. Morcillo, *ChemistryEurope*, 2023, **1**, e202300021.

15 (*a*) J. Han, S. Guo, H. Lu, S. Liu, Q. Zhao and W. Huang, *Adv. Opt. Mater.*, 2018, **6**, 1800538; (*b*) J. Ahn, S. H. Lee, I. Song, P. Chidchob, Y. Kwon and J. H. Oh, *Device*, 2023, **1**, 100176.

16 CCDC 2485128: Experimental Crystal Structure Determination, 2026, DOI: 10.5517/ccdc.csd.cc2pdzfj.